OCTOBER 25 2002

Modal analysis of a drumlike silencer

Lixi Huang

J. Acoust. Soc. Am. 112, 2014–2025 (2002)
https://doi.org/10.1121/1.1508778

Modal analysis of a drumlike silencer

Lixi Huang[a)]
Department of Mechanical Engineering, The Hong Kong Polytechnic University, Kowloon, Hong Kong

(Received 23 January 2002; revised 15 July 2002; accepted 15 July 2002)

Low-frequency duct noise is difficult to deal with by passive methods such as porous duct lining. Reactive methods like expansion chamber are rather bulky, while compact resonators are too narrow banded. This study shows that a suitably stretched thin membrane backed by a slender cavity can achieve a satisfactory performance from low to medium frequencies over an octave band. The present paper focuses on the details of the modal behavior of the fully coupled membrane-cavity system, and examples are given with parameters set in a practical range. Typically, the membrane has a structure to air mass ratio of unity, and is stretched towards the elastic stress limit for a material like aluminum. The backing cavity has a depth equal to the duct height and a length five times the duct height. Three resonant peaks are found in the low to medium frequency range while the transmission loss between adjacent peaks remain above 10 dB. For the first peak, almost complete sound reflection occurs as a result of an out-of-phase combination of the first and second *in vacuo* modes of simply supported membranes. The second peak is solely contributed to by the first mode, while the third peak features mainly the second mode vibration. © *2002 Acoustical Society of America.* [DOI: 10.1121/1.1508778]

PACS numbers: 43.50.Gf, 43.20.Tb, 43.20.Ks [MRS]

I. INTRODUCTION

The objective of this study is to explore a mechanism of broadband, passive control of duct noise without using porous duct lining. Porous media have been the backbone of almost all dissipative noise abatement techniques. It is a very mature and reliable technique which works for a very broad frequency band. But there are two concerns, one acoustical and another environmental. Acoustically, existing sound absorption techniques are ineffective in the low frequency range, such as that below 200 Hz. This range is also often over-looked due to its low A-weighting. Nevertheless, the actual power of noise radiation from, say, a fan, is often highest in this frequency range. Environmentally, there has been increasing concern about the deposition and accumulation of dusts in the pores of the porous material. A periodical cleaning of the lining would be rather costly and indeed tedious. In fact, there are already public concerns of bacteria breeding in the centralized ventilation systems of ordinary commercial buildings. The use of porous material for noise or heat insulation purposes might have contributed to an indoor air quality which is often worse than outdoors. There are also places such as operation theatres, where high hygienic requirement forbids the use of such materials.

The need of controlling low frequency noise in an environment friendly manner calls for a fiberless approach. A team of acousticians led by Fuchs (2001a) have been very successful in achieving this goal, both technically and commercially. The building blocks for their devices include microperforated sheets for sound absorption, and impervious thin membranes for separating the harsh environment from acoustic elements like resonators (Fuchs, 2001b). Active control techniques are also implemented, albeit in its simplest and most practical fashion. Sharing exactly the same goal of fiberless noise control at low-frequencies, the present study sets out to tackle the specific problem of duct noise by yet another approach. Instead of using a thin membrane (such as aluminum of around 0.1 mm thickness) in its natural state, the use of such membranes under high tension is explored. It is found in this study that a grazing incident noise induces the tensioned membrane to vibrate in a low-order axial mode, and such vibration reflects low-frequency noise very effectively. The acoustic elements in the present theoretical model are entirely reactive without any sound absorption material, nor microperforation, although some mechanism of energy dissipation always exists in all experimental rigs. As it turns out, the level of tensile stress required to produce a broadband performance approaches the elastic limit of common materials like aluminum. For this reason, the device is tentatively called a drum silencer. Unlike normal vehicle exhaust silencer or splitter silencers commonly used in the ventilation systems, the drum silencer reflects noise without causing any extra pressure loss.

Focusing on the fundamental mechanism of air-membrane interaction, the present article is devoted to the analysis of membrane response expressed in terms of its *in vacuo* modes. The remaining paragraphs of the introduction are devoted to the theoretical modelling in studies related to the interaction of sound and flexible walls. Knowledge of such interaction has been steadily built up during the past three decades or so. Research in this area has been motivated by a diverse range of engineering problems which include, but are not limited to, aerospace, underwater and room acoustics applications. For example, Lyon (1963), Pretlove (1965), and Guy (1979) studied the effect of a plane flexible wall on the transmission of sound into rooms or cavities. Pan and Bies (1990), and Sum and Pan (1998) investigated the effect of flexible walls on the reverberation performance of rooms. Cheng (1994) investigated the coupling of sound with

a)Electronic mail: mmlhuang@polyu.edu.hk

cylindrical shells simulating aircraft cabins, the purpose being to identify the noisiest structural modes in the cabin. Dowell and Voss (1963), and Dowell *et al.* (1977) studied the stability of a cavity-backed panel exposed to external flows. In all these studies, the pressure on the internal panel surface, i.e., the side facing the cavity, is expanded in terms of the normal cavity modes, and the excitation pressure on the external panel surface is prescribed. In most cases, the cavity air modifies the panel vibration and the mode is said to be panel controlled. On the other hand, when the cavity is very shallow and the excitation frequency is low, the cavity becomes stiffer than the panel, the latter then acts merely as an added mass to the room acoustics mode. This scenario is often categorized as strong fluid-structure interaction when one chooses to regard such modified room modes as an eigenmode of the panel, see, for example, Pretlove (1965). The radiation pressure on the external panel surface is either ignored or lumped into a prescribed excitation force. The validity of such simplification, and the dominance of either fluid or structure in modified modes of resonance, are in fact characteristic of weak coupling in the context of the present studies. The structure used in the current model is a thin membrane with negligible bending stiffness. It is found here that the panel-controlled or cavity-controlled resonance tends to be ineffective as far as the reflection of grazing incident wave is concerned. Another departure of this study from the previous literature is that the radiation pressure on the membrane surface external to the cavity is fully coupled with the membrane motion. This fluid loading is found to be equally important as the acoustic response inside the cavity.

In the field of architectural acoustics, panels are also widely used in front of walls and under the ceilings to enhance the low-frequency sound absorption via the excitation of cavity or panel resonance. Often, these panels also serve optical purposes. To achieve sufficient sound absorption, porous material may be used behind the panel. Perforated panels and multilayer designs may also be employed. Analytical efforts have been made to predict the acoustic performance of such panels. For example, Kang and Fuchs (1999) successfully treated the problem of microperforated membrane as a parallel connection of the (impervious) membrane and apertures. This is a locally reactive model which nevertheless reveals most of the essential physics. Frommhold *et al.* (1994) described the acoustic performance of a splitter silencer made by a host of combined Helmholtz and plate resonators. The analysis is again carried out on the basis of locally reactive model based on the normal incidence impedance of a single resonator. Using the Helmholtz integral formulation, Horoshenkov and Sakagami (2001) studied sound reflection and absorption by a finite, poroelastic plate in an infinite rigid baffle. The plate is supported by a shallow cavity which is filled with sound absorption materials. The cavity is infinite in the direction parallel to the panel. The analytical method employed in this study is rigorous, but the configuration differs from that of the present study where the cavity is enclosed. A recent study conducted by Mechel (2001) dealt with both locally reactive and bulk reactive poroelastic panels supported by an enclosed cavity.

Compared with all the related studies mentioned above, the theoretical model and the solution method described in the present paper have the following distinct features: (a) the membrane and the cavity are finite but not necessarily compact; (b) there is no simplification assumption made regarding the radiation pressure on either side of the membrane; (c) the pressure on the panel surface facing the cavity is expressed in terms of the duct acoustics modes instead of the room acoustics modes. Multiple resonant peaks are found and, when an appropriate combination of cavity and membrane properties are chosen, the breakdown of transmission loss between these peaks is moderate, and a level of 10 dB is sustained for a continuous frequency range wider than an octave band. This represents an attractive performance considering the fact that an expansion chamber of the same cavity size yields a maximum transmission loss of 5 dB when it experiences a quarter wavelength resonance. In what follows, Sec. II outlines the analytical formulation for the membrane response to a grazing incident wave. Section III gives the spectra of transmission loss as well as details of all modal interactions for a typical example which can be easily materialized. Section IV focuses on the wave-reflecting behavior of the coupled system at the low frequency region, where an approximate and closed-form solution is possible. Qualitative analysis is extended to moderate frequencies where the transmission loss attains peak values. The main physical ingredients are summarized in the conclusion section.

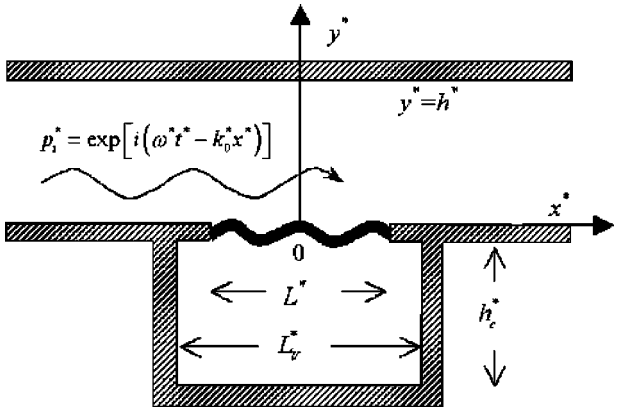

FIG. 1. Configuration of the theoretical model.

II. METHOD OF SOLUTION

The configuration is shown in Fig. 1. It has a two-dimensional duct, or channel, of height h^*, lined in part by a membrane of length L^* on the lower wall. The asterisks denote dimensional variables while the corresponding dimensionless ones are introduced shortly without asterisks. The membrane is simply supported at the two edges, $|x^*| = L^*/2$, and is enclosed by a rigid-walled cavity of depth h_c^* and length L_v^*. L_v^* is held equal to L^* in the numerical example to be given later, but a general formulation for $L_v^* > L^*$ is sought for the sake of parametric studies on the shape of the cavity. The question now is how the membrane responds to an incident wave of unit amplitude, $p^{*\prime} = \exp[i(\omega^* t^* - k_0^* x^*)]$, where $\omega^* = 2\pi f^*$ and $k_0^* = \omega^*/c_0^*$ are, respectively, the angular frequency and the wave number based on the speed of sound in free space, c_0^*. The flexible

wall has a mass per unit length m^*, and a tensile force T^* is applied. The governing equation for the membrane vibration is

$$m^*\frac{\partial^2 \eta^*}{\partial (t^*)^2} - T^*\frac{\partial^2 \eta^*}{\partial (x^*)^2} + (p_+^* - p_-^*) = 0, \tag{1}$$

where η^* is the membrane displacement, and $(p_+^* - p_-^*)$ is the fluid loading on the membrane located at $y^* = 0$. Positive loading means a net force acting downwards, and positive modal impedance, which is introduced shortly, refers to positive loading induced by an upward membrane vibration velocity. Structural damping in a thin membrane like this is normally small and is excluded at present, so is bending stiffness. Dividing Eq. (1) by $\rho_0^*(c_0^*)^2$, where ρ_0^* is the fluid density, yields

$$\frac{m^*}{\rho_0^* h^*}\frac{\partial^2(\eta^*/h^*)}{\partial(t^* c_0^*/h^*)^2} - \frac{T^*}{h^*\rho_0^*(c_0^*)^2}\frac{\partial^2(\eta^*/h^*)}{\partial(x^*/h^*)^2} + \frac{p_+^* - p_-^*}{\rho_0^*(c_0^*)^2} = 0. \tag{2}$$

All variables are now nondimensionalized as follows by three basic quantities, ρ_0^*, h^*, and c_0^*:

$$x = \frac{x^*}{h^*}, \quad y = \frac{y^*}{h^*}, \quad t = \frac{c_0^* t^*}{h^*},$$

$$h_c = \frac{h_c^*}{h^*}, \quad f = \frac{f^* h^*}{c_0^*}, \quad \omega = \frac{\omega^* h^*}{c_0^*}, \tag{3}$$

$$k_0 = 2\pi f, \quad m = \frac{m^*}{\rho_0^* h^*}, \quad T = \frac{T^*}{h^*\rho_0^*(c_0^*)^2}, \quad p = \frac{p^*}{\rho_0^*(c_0^*)^2}.$$

m is the mass ratio and T is the dimensionless tensile force. In a real, three-dimensional laboratory model, T is calculated by dividing the total force applied on the membrane by $\rho_0^*(c_0^*)^2 A^*$, where A^* is the cross section of a rectangular duct. Note that $\omega = k_0$ according to the above normalization scheme. The first cut-on frequency of the duct is $f = 0.5$. Equation (2) becomes

$$m\frac{\partial^2 \eta}{\partial t^2} - T\frac{\partial^2 \eta}{\partial x^2} + (p_+ - p_-) = 0. \tag{4}$$

Note that, in reality, the two-dimensional model can only be realized properly when the duct has a finite width in the third direction, say $z \in [0, h_z]$, and the width h_z cannot be too wide as to cause higher order modes in that direction. Meanwhile, the membrane should be allowed to move freely at the edges of $z = 0+$, h_z- with a tiny gap with the duct walls. The solution for a simplified model excluding the cavity effect was given in Huang (1999). The same procedure is followed here. The main steps are described very briefly and issues unique to the current model are discussed in more details.

For harmonic vibrations, and introducing membrane vibration velocity $V = \partial\eta/\partial t = i\omega\eta$, Eq. (4) becomes

$$mi\omega V - (T/i\omega)\partial^2 V/\partial x^2 + (p_+ - p_-) = 0. \tag{5}$$

Equation (5) can be solved via the standard Galerkin procedure, in which V is expanded as a series of *in vacuo* modes with modal amplitude V_j,

$$V_j(t) = 2\int_0^1 V(x,t)\sin(j\pi\xi)\,d\xi, \tag{6}$$

where

$$\xi = x^*/L^* + 1/2, \tag{7}$$

is the local axial coordinate. Equation (5) then becomes

$$\mathcal{L}_j V_j + 2\int_0^1 (p_+ - p_-)\sin(j\pi\xi)\,d\xi = 0,$$
$$\mathcal{L}_j = \left[mi\omega + \frac{T}{i\omega}\left(\frac{j\pi}{L}\right)^2 \right], \quad j = 1,2,3,\ldots. \tag{8}$$

A. Radiation and cavity reflection impedances

Traditionally, the fluid loading inside the cavity, p_-, is found by cavity modes while the upper surface loading, p_+, is specified as part of the external excitation force. This approach is invalid for the current problem since the coupling of air and membrane motion is very strong. For this reason, it is more convenient to take the following approach. The fluid loading, $(p_+ - p_-)$, is divided into three parts. Part one is the upper surface pressure due to the specified incident wave without considering the membrane response,

$$p_i(x,t) = \exp[i(\omega t - k_0 x)]. \tag{9}$$

Part two is the sound radiated by the membrane vibration excluding the reflections by the vertical walls of the cavity located at $|x| = L_v/2$. The radiation pressure on the lower side, denoted as $p_{-\mathrm{rad}}$, is formulated in a way similar to that in the main duct, $p_{+\mathrm{rad}}$. In the special case where $h_c = 1$, it is shown that $p_{-\mathrm{rad}} = -p_{+\mathrm{rad}}$, and the pressure difference is simply twice the radiation pressure on the upper side. The third part is due to the reflection from the two vertical cavity walls, denoted as $p_{-\mathrm{ref}}$. Hence,

$$(p_+ - p_-) = p_i + (p_{+\mathrm{rad}} - p_{-\mathrm{rad}}) - p_{-\mathrm{ref}}. \tag{10}$$

The radiation pressure in the main duct is well known (Doak, 1973), and is written here in the dimensional form first. The pressure consists of contributions from all duct acoustics modes of index n,

$$p_{+\mathrm{rad}}^*(x^*,y^*,t^*) = \frac{\rho_0^*}{2h^*}\sum_{n=0}^{\infty} c_n^*\psi_n(y^*) \times \int_{-L^*/2}^{+L^*/2} \psi_n^*(y^{*\prime}) V^*(x^{*\prime},y^{*\prime},t^*) \times [H(x^*-x^{*\prime})e^{-ik_n^*(x^*-x^{*\prime})} + H(x^{*\prime}-x^*)e^{+ik_n^*(x^*-x^{*\prime})}]\,dx^{*\prime}, \tag{11}$$

where H is the Heaviside function, c_n^*, k_n^*, and ψ_n^* are, respectively, the modal phase speed, the modal wave number, and the modal velocity potential,

$$c_n^*=\frac{ic_0^*}{\sqrt{(n\pi c_0^*/\omega^* h^*)^2-1}},\quad k_n^*=\frac{\omega^*}{c_n^*},$$
$$\psi_n^*(y^*)=\sqrt{2-\delta_{0n}}\cos(n\pi y^*/h^*), \tag{12}$$

and δ_{0n} is the Kronecker delta. Equation (11) is valid for any time history and location of the source V^*. From this point onwards, the source is specified as a harmonic membrane vibration at $y^{*\prime}=0$, $x^{*\prime}\in[-L^*/2,L^*/2]$. All variables are represented by their amplitudes, such as $p^*_{+\mathrm{rad}}(x^*,y^*)$ and $V^*(x^{*\prime})$. There are two important length scales, one is h^* and another is L^*. The former concerns the duct acoustics modes while the latter concerns the membrane dynamics. The local dimensionless coordinate ξ introduced in Eq. (7) is used together with x, and ξ' with x'. The dimensionless radiation pressure can be established from Eq. (11),

$$p_{+\mathrm{rad}}(x,y)=\frac{L}{2}\sum_{n=0}^{\infty}c_n\psi_n(y)\int_0^1\psi_n(y')V(x')\times[H(x-x')e^{-ik_n(x-x')}+H(x'-x)e^{+ik_n(x-x')}]d\xi'. \tag{13}$$

The dimensional Eq. (11) allows easy translation of Eq. (13) into the lower duct where the relevant duct acoustics scale is h_c^* and the membrane scale remains as L^*. The radiation pressure inside the cavity for the general case of $h_c^*\neq h^*$ is

$$p_{-\mathrm{rad}}(x_c,x_c)=\frac{L_c}{2}\sum_{n=0}^{\infty}c_{nc}\psi_n(y_c)\int_0^1\psi_n(y_c')[-V(x_c')]\times[H(x_c-x_c')e^{-ik_{nc}(x_c-x_c')}+H(x_c'-x_c)e^{+ik_{nc}(x_c-x_c')}]d\xi', \tag{14}$$

where the quantities peculiar to the cavity are distinguished by an additional subscript c as defined below:

$$x_c=\frac{x^*}{h_c^*},\quad y_c=\frac{y^*}{h_c^*},\quad L_c=\frac{L^*}{h_c^*},\quad L_v=\frac{L_v^*}{h_c^*},$$
$$\omega_c=\frac{\omega^* h_c^*}{c_0^*}=\omega h_c,\quad c_{nc}=\frac{i}{\sqrt{(n\pi/\omega_c)^2-1}},\quad k_{nc}=\frac{\omega_c}{c_{nc}}. \tag{15}$$

The reflection in the cavity is calculated in a form similar to the radiation pressure (14) except that the Heaviside functions are replaced by unknown coefficients A and B. The reflection for sound radiated by an elemental source of length $d\xi'$ is

$$dp_{-\mathrm{ref}}=\frac{L_c}{2}\sum_{n=0}^{\infty}c_{nc}\psi_n(y)\psi_n(y')\times[Ae^{-ik_{nc}(x_c-x_c')}+Be^{+ik_{nc}(x_c-x_c')}][-V(x_c')]d\xi',$$

where A and B are determined by the rigid wall boundary conditions,

$$\left.\frac{\partial(p_{-\mathrm{rad}}+p_{-\mathrm{ref}})}{\partial x_c}\right|_{|x_c|=L_v/2}=0,$$

to be satisfied for each duct acoustics mode n. Hence,

$$(1+B)e^{ik_{nc}(-L_v/2-x_c')}-Ae^{-ik_{nc}(-L_v/2-x_c')}=0,$$
$$-(1+A)e^{-ik_{nc}(L_v/2-x_c')}+Be^{ik_{nc}(L_v/2-x_c')}=0.$$

Solving these two equations yields

$$A=\frac{e^{ik_{nc}(L_v-2x_c')}+1}{e^{ik_{nc}(2L_v)}-1},\quad B=\frac{e^{ik_n(L_v+2x_c')}+1}{e^{ik_n(2L_v)}-1},$$

hence the reflection pressure

$$p_{-\mathrm{ref}}(x_c,y_c)=\frac{L_c}{2}\sum_{n=0}^{\infty}c_{nc}\psi_n(y_c)\int_0^1\psi_n(y_c')[-V(x_c')]\times\frac{2}{e^{ik_{nc}(2L_v)}-1}[\cos k_{nc}(x_c-x_c')+e^{ik_{nc}L_v}\cos k_{nc}(x_c+x_c')]d\xi'. \tag{16}$$

In order to solve the membrane dynamics, Eq. (8), the fluid loading (p_+-p_-) has to be related to the modal vibration velocity amplitudes V_j by the following modal decomposition:

$$(p_+-p_-)=\sum_{j=1}^{\infty}V_j p_j^1(x),$$

where $p_j^1(x)$ is the fluid loading caused by the modal vibration of unit amplitude, $V=\sin(j\pi\xi)$, which is to be substituted into Eqs. (13) and (16). The resulting loading contains not only the source mode of index j, but also of all other modes. Modal impedance is now defined as

$$Z_{jl}=\int_0^1 2\sin(l\pi\xi)p_j^1(x,0)d\xi,$$

where subscript j refers to the source vibration mode while l the resulting pressure coefficient. Part of Z_{jl} derives from $p_{+\mathrm{rad}}$ which was given in Huang (1999), and is now given the new symbol of Z_{+jl}. The contribution from the lower side of the membrane is denoted as Z_{-jl}, while that caused by the vertical wall reflections as Z_{rjl}. The total modal impedance Z_{jl} is calculated as follows:

$$Z_{jl}=Z_{+jl}+Z_{-jl}+Z_{rjl}=\int_0^1 2\sin(l\pi\xi)(p_{+\mathrm{rad}}-p_{-\mathrm{rad}}-p_{-\mathrm{ref}})_j^1\,d\xi. \tag{17}$$

Z_{+jl} given in Huang (1999) can be recovered here from Z_{-jl} by specifying $h_c=1$. The results for Z_{-jl} and Z_{rjl} are

$$Z_{-jl}=L_c\sum_{n=0}^{\infty}c_{nc}(2-\delta_{0n})\mathcal{I}_{2c}(n,j,l),$$
$$Z_{rjl}=L_c\sum_{n=0}^{\infty}c_{nc}(2-\delta_{0n})\mathcal{I}_{2r}(n,j,l), \tag{18}$$

where $\mathcal{I}_{2c}$ and $\mathcal{I}_{2r}$ are the results of double-integration over the membrane surface,

$$\mathcal{I}_{2c}(n,j,l)=\frac{l\pi j\pi(\cos j\pi-e^{-ik_{nc}L_c})(\cos j\pi+\cos l\pi)}{[(j\pi)^2-(k_{nc}L_c)^2][(l\pi)^2-(k_{nc}L_c)^2]}+\frac{ik_{nc}L_c\delta_{jl}}{(j\pi)^2-(k_{nc}L_c)^2}, \tag{19}$$

$$\mathcal{I}_{2r}(n,j,l)=\frac{2j\pi l\pi(1-\cos j\pi\cos k_{nc}L_c)(\cos j\pi-e^{ik_{nc}L_v})(\cos j\pi+\cos l\pi)}{[(j\pi)^2-(k_{nc}L_c)^2][(l\pi)^2-(k_{nc}L_c)^2][e^{-ik_{nc}(2L_v)}-1]}. \tag{20}$$

Two observations are made. First, the results for $\mathcal{I}_{2c}(n,j,l)$ and $\mathcal{I}_{2r}(n,j,l)$ vanish when j is even and l is odd, or when l is even and j is odd. This property decouples the even and odd modes of the membrane, and all subsequent analytical processing is focused on the case of $\cos j\pi=\cos l\pi$. The second observation is that, when $k_{nc}L_c$ coincides with $j\pi$ or $l\pi$, $\mathcal{I}_{2c}(n,j,l)$ becomes 0/0-type, and the finite results are similar to those for Z_{+jl} given in Huang (1999). The only possible mode which may cause this is the plane wave mode $n=0$, unless the cavity is very deep and the incident wave has higher order modes in the cavity. When $L_v=L$, and $k_{0c}L_v\to\ell\pi$, where ℓ is also an integer, the cavity reflection term $\mathcal{I}_{2r}$ may diverge,

$$\lim_{k_{nc}L_v\to\ell\pi}\mathcal{I}_{2r}(0,j,l)=\begin{cases}\infty, & \text{when } (-1)^\ell=-(-1)^j=-(-1)^l;\\ -i/2, & \text{when } \ell=j=l;\\ 0, & \text{otherwise.}\end{cases} \tag{21}$$

This implies that, for a duct length equal to an odd multiple of half wavelength, it's impossible to excite the even modes on the membrane.

B. Membrane response and transmission loss

Having found the modal radiation and cavity reflection impedances, the dynamics Eq. (8) can be cast as a truncated set of linear equations for the modal vibration amplitudes, V_j, $j=1,2,3,...,N$,

$$\begin{bmatrix}Z_{11}+\mathcal{L}_1 & Z_{12} & \cdots & Z_{1N}\\ Z_{21} & Z_{22}+\mathcal{L}_2 & \cdots & Z_{2N}\\ \cdots & \cdots & \cdots & \cdots\\ Z_{N1} & Z_{N2} & \cdots & Z_{NN}+\mathcal{L}_N\end{bmatrix}\begin{bmatrix}V_1\\V_2\\V_3\\\vdots\\V_N\end{bmatrix}+\begin{bmatrix}I_1\\I_2\\I_3\\\vdots\\I_N\end{bmatrix}=0, \tag{22}$$

where I_j is the modal coefficient of the incident wave,

$$I_j=\int_0^1 p_i 2\sin(j\pi\xi)d\xi=2j\pi e^{ik_0L/2}\left[\frac{1-e^{i(-k_0L+j\pi)}}{(j\pi)^2-(k_0L)^2}\right]. \tag{23}$$

Note that $N=25$ is normally enough as further increase in N does not make any noticeable difference.

The final transmitted wave is found by adding the incident wave, p_i, to the far-field radiation wave, $p_{+\mathrm{rad}}$, which can be found from Eq. (13) taking only the plane wave mode $n=0$ for $x>L/2$:

$$p_t=p_{+\mathrm{rad}}|_{n=0,x\to+\infty}+p_i. \tag{24}$$

For an incident wave of unit amplitude, $|p_i|=1$, the transmission loss is calculated as

$$\mathrm{TL}=-20\log_{10}|p_t|. \tag{25}$$

Denoting the reflected sound as $p_re^{ik_0x}$, the coefficients of sound power reflected and absorbed, if there is structural damping, are calculated as follows:

$$\beta=|p_r|^2,\quad \alpha=1-|p_r|^2-|p_t|^2. \tag{26}$$

When two identical membrane-cavity systems are used, one at each side of a two-dimensional channel, the two membranes can be shown to respond in an identical manner. The pressure loading on the upper side of the lower membrane, $p_{+\mathrm{rad}}$, must account for that caused by the opposite membrane, which is the same as the reciprocal pressure on $y=1$ caused by the lower membrane. The latter can be calculated by setting $y=1$ in $\psi_n(y)$ in Eq. (13). The performance of a two-membrane configuration can also be calculated by regarding the channel height as $h^*/2$, but caution must be taken to avoid mistakes when converting the results back to the dimensionless form based on the full duct height h^*.

The complex amplitude of the reflected sound, p_r, is the sum of contributions made by all individual membrane vibration modes, which is found as follows with the help of Eq. (13):

$$p_r=\frac{p_{+\mathrm{rad}}|_{n=0,x\to-\infty}}{e^{ik_0x}}=\frac{1}{2}\int_{-L/2}^{+L/2}V(x')e^{ik_0x'}\,dx'=\sum_{j=1}^{\infty}V_jR_j, \tag{27}$$

where R_j is the complex amplitude of the reflected sound by the induced vibration of the jth mode with unit amplitude,

$$R_j=\frac{1}{2}\int_{-L/2}^{+L/2}\sin(j\pi\xi')e^{-ik_0x'}\,dx'=I_jL/4, \tag{28}$$

and the last identity is found by comparing the integration with that in Eq. (23). As each complex number can be represented by a vector in the real-imaginary space, the contribution of each single mode, denoted as $\mathbf{V}_j\mathbf{R}_j$, towards the total reflected sound, $\mathbf{p}_r$, can be found by projecting the former to the latter as illustrated in Fig. 2. The result is called the modal reflection contribution, γ_j, which is defined below together with the interference index, $\Gamma_{1,2}$, between the contributions from the two modes,

$$\gamma_j=\mathrm{Re}[V_jR_j\hat{p}_r/|p_r|],\quad \Gamma_{1,2}=\cos(\theta), \tag{29}$$

where $\hat{p}_r$ is the conjugate of p_r, and θ is shown in Fig. 2. Note that γ_j is a real scalar, and is a fraction of $|V_jR_j|$. Note also that the magnitudes of both V_j and R_j can be greater than unity, but that of the reflected wave, $p_r=\Sigma_jV_jR_j$, is

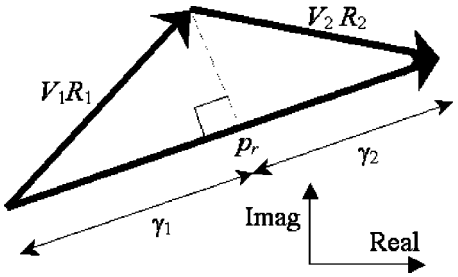

FIG. 2. Projection of reflection caused by each individual mode onto the sum vector $\mathbf{p}_r$.

less than unity since the reflected sound power derives from the incident wave which has a specified magnitude of unity.

III. SPECTRA OF MODAL INTERACTIONS

The results of the overall spectra are presented before the physics of modal response for specific frequencies are discussed. The following set of parameters are used as the default values for a device with two identical membranes, one on each side,

$$m=1, \quad T=0.475, \quad h_c=1, \quad L=L_v=5. \tag{30}$$

The mass ratio is considered to be in the practical range as illustrated by the example of 0.077 mm thick aluminum foil used in a duct of height 170 mm, $m=2700\times0.077/(1.225\times170)=1$. The dimensionless tensile force $T=0.475$ translates into a dimensional force of

$$F^*=T\rho_0^*(c_0^*h^*)^2=0.475\times1.225\times(340\times0.17)^2=1944N$$

for a square duct and the corresponding tensile stress is 148.5 MPa, which is close to but still within the yielding strength of the material. The choice of $h^*=170$ mm as the example is based on the convenience of the frequency unit: $c^*/h^*=2$ kHz, which falls right on the center of octave bands in practical use. The first cut-on frequency for a rigid duct of height 170 mm is thus 1 kHz, and the dimensionless lower stopband to be shown below, $f=0.054$, corresponds to $f^*=108$ Hz. The choice of the default set of parameters in Eq. (30) derives from a parametric study of which a brief summary is given in the conclusions section.

A. Stopband and spectral peaks

The main objective of the study is to see whether a tensioned membrane can achieve a broad stopband, preferably in the low-frequency range. The stopband here is defined as the frequency range, $f\in[f_1,f_2]$, in which TL $\geqslant$10 dB. The cost function for the optimization is set as the ratio of the band limits, f_2/f_1, namely the logarithmic bandwidth. The reason why 10 dB is chosen is the following. When the membranes are removed, the cavities, one on each side, form an expansion chamber of area ratio $(1+2h_c)=3$. The best performance of sound reflection by this reference expansion chamber is about TL=5 dB. It is felt that TL=10 dB would represent a substantial improvement. It is possible that the performance of cavities filled with sound absorption materials might be even better than 10 dB at moderate to high frequencies, but the emphasis of the current study is on the control of low-frequency noise. Most of the

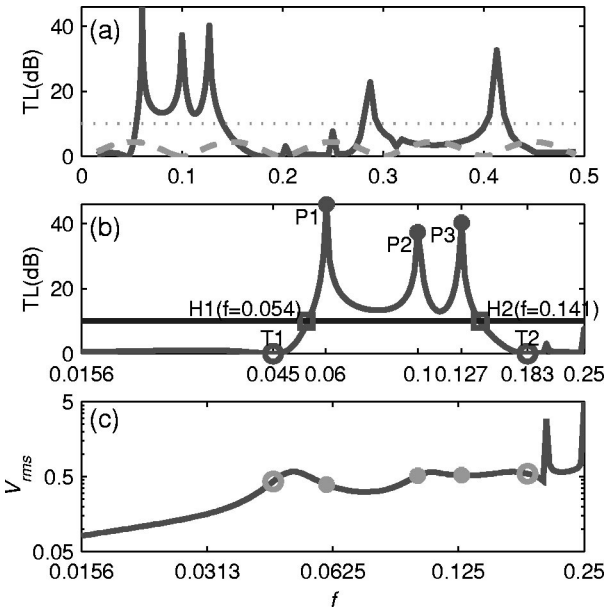

FIG. 3. Performance of two opposite membranes under tension $T=0.475$. The dashed curve in (a) is for a simple expansion chamber with an area ratio of $(1+2h_c)=3$. The peaks are illustrated by ● and the troughs by ○.

following analyses show a spectrum over four octaves. The frequency of four octaves down from $f=0.5$ is $0.5/2^4=0.0313$, which is 62.5 Hz for the above example of the 170 mm duct.

Figure 3 shows the results for the default configuration specified in (30). The scale of frequency in Fig. 3(a) is linear, and it covers the whole plane wave frequency for the rigid channel, $f\in(0,0.5)$. The horizontal dashed line is the threshold level 10 dB. The dashed curve in Fig. 3(a) is drawn for the plane-wave theory of the expansion chamber of an area ratio of 3. A wide stopband is found in the low frequency range below $f=0.15$, which is the range of focus for the present study. Figures 3(b) and (c) use a logarithmic scale for the four octave frequency band from $f=0.0156$ to 0.25. The ranges of frequencies shown in these two subfigures are identical, but in Fig. 3(b) the frequencies of troughs and peaks are labeled for easy reference. Figure 3(b) shows that the stopband begins from $f_1=0.054$ (marked as point H1) and ends at $f_2=0.141$ (marked as point H2), the ratio being $f_2/f_1=2.6$. Three peaks are marked in both Fig. 3(b) and Fig. 3(c), by asterisks and labeled as P1, P2, and P3. Two troughs are identified as open circles, and labeled as T1 and T2, respectively. Figure 3(c) shows a gradually increasing rms level of the membrane response calculated by $V_{\rm rms}=(\Sigma_j|V_j|^2/2)^{1/2}$. The vertical coordinate is logarithmic to show more detail features. The important observation here is that the peaks and troughs do not correspond to the level of high or low membrane response, as shown by the lack of correlation between the marked peaks and troughs with the actual variation pattern of $V_{\rm rms}$. In other words, the effectiveness of the membrane to reflect sound does not solely depend on the amplitude of the induced membrane vibration. As is shown later, it mainly depends on the acoustic interference of sound radiated by different parts of the membrane. Since the membrane vibration is decomposed into axial modes of *in vacuo* membrane vibration, $\sin(j\pi\xi)$, it is con-

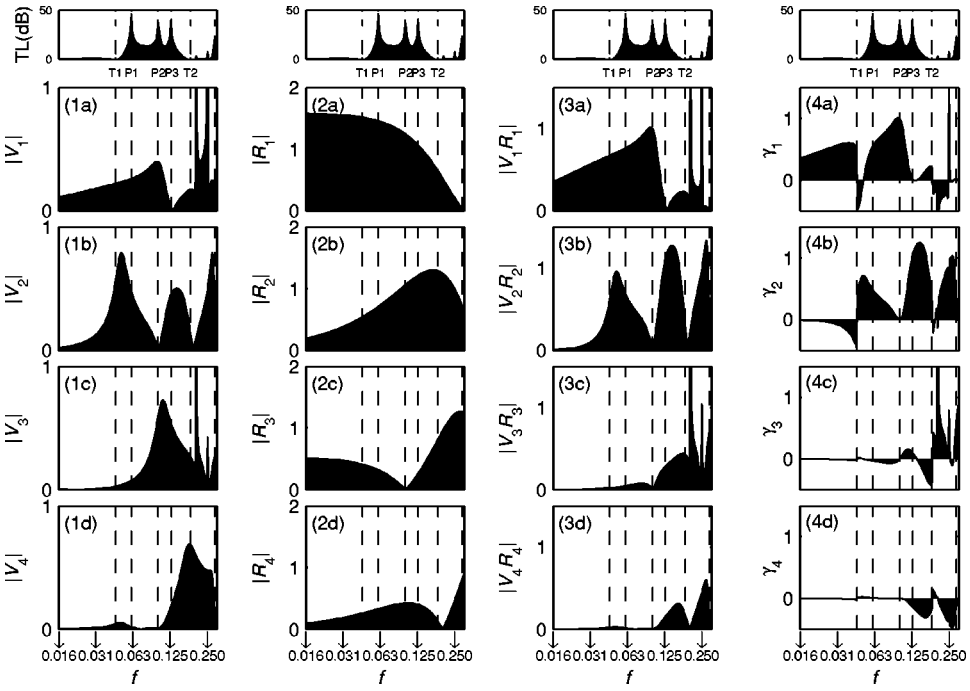

FIG. 4. Modal reflections. The first column on the left is for the modal amplitude, $|V_j|$, the second column is for the modal reflection coefficient, $|R_j|$, the third column is for the single mode reflection $|V_jR_j|$, and the last column on the right is for the modal contribution γ_j defined in Fig. 2. The top row is the TL spectrum for the purpose of identifying important frequencies.

venient to investigate the interference pattern in terms of these modes.

B. Modal reflections

The modal response for the default membranes is shown in Fig. 4. The vibration amplitude of each individual mode, $|V_j|$, is shown in the subfigures on the left column. A TL spectrum is attached on top of each column to facilitate the correlation study between the peak and trough frequencies analyzed in Fig. 3, and the modal response. The second column is the amplitude of the modal sound reflection coefficient, $|R_j|$, which is also related to the modal loading of the incident wave I_j by $R_j = I_j L/4$, cf. Eqs. (28) and (23). The third column is the amplitude of the single mode reflection, $|V_jR_j|$. The fourth column shows the modal contribution towards the total sound reflection, γ_j, defined in Eq. (29).

The membrane resonance points are analyzed first. As shown in Fig. 4(1a), there are two sharp peaks in the first mode amplitude, $|V_1|$, one next to the frequency of T2, and one right on the border frequency of $f=0.25$. There is also a 3rd mode peak, $|V_3|$, shown in Fig. 4(1c). These peaks are also seen in the response curve of Fig. 3(c). It might be tempting to relate these frequencies with conditions where the membrane length is equal to the multiples of the incident wavelength or the quarter wavelength, but such simple analysis does not hold since these frequencies change with tension. The two frequency points certainly represent membrane resonance (to be discussed later), but such resonance does not produce much sound reflection since TL is not high at these frequencies. The reason why TL is low can be found from the figures in the fourth column. Taking $f=0.2$ as an example, there is a sharp negative peak in Fig. 4(4a), which is clipped in the figure, and a sharp positive peak in Fig. 4(4c). Both modal ineffectiveness and intermodal cancellation are manifestations of destructive acoustic interference of sound radiated by different portions of the membrane. Details of the modal response for the first two modes and the specific frequency points where TL is high are analyzed in the next section.

The degree of intermodal coupling can be seen in the left column of Fig. 4. For example, in the frequency range below about 0.05, $|V_3|$ shown in 4(1c) is much smaller than $|V_1|$ shown in Fig. 4(1a). Therefore, a single mode analysis can be conducted for the first mode below $f=0.05$. Beyond this point, the coupling effect is strong and a detailed analysis becomes difficult and less rewarding. For the coupling between the second and the fourth modes shown in Figs. 4(1b) and (1d), single mode analysis can be conducted for the second mode below $f=0.1$. Further analysis is concentrated in these low-frequency ranges where the cross-modal coupling is weak.

IV. LOW FREQUENCY AND PEAK POINTS

Within the frequency range where the first two modes are decoupled from the higher order modes, it is possible to find a closed-form solution and reveal the functional relationship for important features of the coupled system. For this purpose, the core expressions of modal impedances shown in Eqs. (19) and (20) are analyzed here for both odd-odd and even-even combinations of modal indices, j, l. Introducing the following membrane and cavity parameters:

$$\theta_n = k_{nc}L_c, \quad \theta \equiv \theta_0 = k_{0c}L_c = k_0 L, \quad \Theta = k_{0c}L_v, \qquad (31)$$

and recalling from Eq. (18),

$$Z_{-jl} = L_c \mathcal{I}_{2c}(0,j,l) + 2\sum_{n=1}^{\infty} c_{nc}\mathcal{I}_{2c}(n,j,l),$$

$$\mathcal{I}_{2c}(n,j,l) = \frac{2j\pi l\pi[1-e^{ij\pi - i\theta_n}]}{[(j\pi)^2-\theta_n^2][(l\pi)^2-\theta_n^2]} + \frac{i\theta_n\delta_{jl}}{(j\pi)^2-\theta_n^2},$$

where c_{nc}, $k_{nc}L_c$ for the higher order duct modes are purely imaginary and can be approximated as follows:

$$c_{nc}=\frac{i}{\sqrt{(n/2f)^2-1}}\approx\frac{i2f}{n},$$

$$\theta_n=k_{nc}L_c\approx\frac{2\pi f}{i2f/n}L_c=-in\pi L_c.$$

Since $|c_{nc}|$ is very small and $|\theta_n|$ very large, the denominator $[(j\pi)^2-(\theta_n)^2]\approx[(L_cn\pi)^2+(j\pi)^2]$ diverges as $(L_cn)^2$ as n increases. The two terms in $\mathcal{I}_{2c}$ $(n>0,j,l)$ diverge as $(L_cn)^{-4}$ and $(L_cn)^{-1}$, respectively. Numerical analysis shows that, for the typical parameters set in Eq. (30), the higher order modes $\mathcal{I}_{2c}$ $(n>0,j,l)$ contribute little to the radiation impedance Z_{-jl}. It is therefore only necessary to concentrate on the plane wave mode, $n=0$. The same conclusion holds for the reflection impedance Z_{rjl}.

A. Plane wave approximation

The plane wave approximation, which neglects all higher order duct acoustics modes, gives

$$Z_{-jl}\approx L_c\left[\frac{2jl\pi(1-e^{il\pi-i\theta})}{[(j\pi)^2-\theta^2][(l\pi)^2-\theta^2]}+\frac{i\theta\delta_{jl}}{(j\pi)^2-\theta^2}\right],$$

$$Z_{rjl}\approx L_c\frac{8jl\pi(1-\cos j\pi\cos\theta)(1-e^{i\Theta+ij\pi})}{[(j\pi)^2-\theta^2][(l\pi)^2-\theta^2][e^{i2\Theta}-1]}.$$

For $L=L_v=5$, and $f=0.0156$, 0.0313, 0.0625, 0.125, $\theta=\Theta$ is, respectively, 0.491, 0.982, 1.964, and 3.927. In the frequency range where the first two modes are quite decoupled from the higher order modes, as discussed before this section, the solutions to the dynamics Eq. (22) are simply

$$V_1\approx\frac{-I_1}{(Z_{11}+\mathcal{L}_1)},\quad V_2\approx\frac{-I_2}{(Z_{22}+\mathcal{L}_2)}.$$

For a configuration in which there are two identical membranes and accounting only the duct acoustics mode of $n=0$, the total modal impedance is $Z=(2Z_{+\mathrm{rad}}+Z_{-\mathrm{rad}})+Z_{-\mathrm{ref}}$. The plane wave approximation of Z_{11} is

$$Z_{11}=(L_2+2L)\left[\frac{2\pi^2(1+e^{-i\theta})}{[\pi^2-\theta^2]^2}+\frac{i\theta}{\pi^2-\theta^2}\right]-2L_c\frac{2\pi^2(1+\cos\theta)}{[\pi^2-\theta^2]^2[1-e^{i\Theta}]},$$

where the last group is from $Z_{-\mathrm{ref}}$, which can be further divided into resistance and reactance term by

$$\frac{1}{1-e^{i\Theta}}=\frac{1-\cos\Theta+i\sin\Theta}{2-2\cos\Theta}=\frac{1}{2}+\frac{i}{2}\cot\frac{\Theta}{2}.$$

It can be shown that the radiation resistance in the cavity is cancelled out by the real part of the cavity reflection impedance, so that

$$Z_{11}=\overbrace{\left[(2L)\frac{2\pi^2(1+\cos\theta)}{[\pi^2-\theta^2]^2}\right]}^{\text{Radiation resistance}}-\overbrace{i(L_c+2L)\left[\frac{2\pi^2\sin\theta}{[\pi^2-\theta^2]^2}-\frac{\theta}{\pi^2-\theta^2}\right]}^{\text{Radiation reactance (stiffness)}}-\overbrace{iL_c\left[\frac{2\pi^2(1+\cos\theta)}{[\pi^2-\theta^2]^2\tan(\Theta/2)}\right]}^{\text{Cavity reflection reactance (stiffness)}}.\tag{32}$$

Similarly,

$$Z_{22}=\overbrace{\left[(2L)\frac{8\pi^2(1-\cos\theta)}{[(2\pi)^2-\theta^2]^2}\right]}^{\text{Radiation resistance}}+\overbrace{i(L_c+2L)\left[\frac{8\pi^2\sin\theta}{[(2\pi)^2-\theta^2]^2}+\frac{\theta}{(2\pi)^2-(\theta)^2}\right]}^{\text{Radiation reactance (mass)}}+\overbrace{iL_c\left[\frac{8\pi^2(1-\cos\theta)\tan(\Theta/2)}{[(2\pi)^2-\theta^2]^2}\right]}^{\text{Cavity reflection reactance (mass)}}.\tag{33}$$

Notice that, when $\Theta<\pi$, the imaginary part of Z_{11} presents stiffness, but that of Z_{22} a mass. The magnitude of the reactance is small for Z_{22} when $\theta\to0$, but that of Z_{11} diverges like any spring stiffness, and the divergent term is from the cavity reflection. When $\Theta>\pi$, the reverse is true. When Θ passes π, $\tan(\Theta/2)\to\infty$, the cavity has zero stiffness to the first mode but infinite stiffness for the second mode. From this point onwards, Θ is assumed to be the same as θ.

The accurate values of the two impedances are shown in Fig. 5 with sources of contributions marked along the curves.

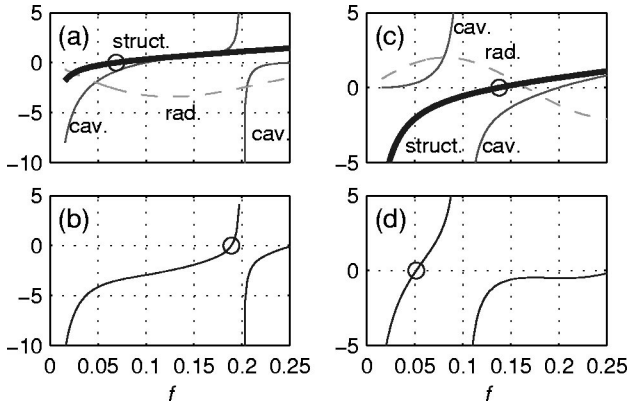

FIG. 5. Reactance of the first two modes and resonant frequencies. (a) shows the components of the first mode reactance. The components are from radiation (marked rad), cavity reflection (marked cav), and structural properties (struct). The open circle marks the frequency of the first *in vacuo* eigen frequency. (b) shows the total reactance for which the zero reactance is also marked by an open circle. (c) shows the second mode components where the second *in vacuo* eigen frequency is marked by an open circle. (d) shows the total reactance of the second mode, where the open circle marks the frequency where the total reactance vanishes.

The two subfigures on the left-hand side are for the first mode reactance including the structural contribution, $\mathrm{Im}(Z_{11}+\mathcal{L}_1)$, while those on the right-hand side for the second mode, $\mathrm{Im}(Z_{22}+\mathcal{L}_2)$. The dashed lines in Fig. 5(a) and Fig. 5(c) are for the radiation components, which are not remarkable except that the second mode radiation reactance vanishes at $f=0.166$. The thin solid lines in these two subfigures are for the cavity reflection reactance. The reactance diverges at the cavity modes where the cavity length is a multiple of the half wavelength, $\theta=j\pi$, $f=0.1,0.2$, $j=2,1$. The two thick solid lines are the structural dynamics contribution which is the combination of inertia and stiffness terms. The open circles indicate the *in vacuo* membrane modes at frequencies $f=(j\pi/L)\sqrt{T/m}=0.069$, 0.138 for $j=1,2$, respectively. Figures 5(b) and (d) show the total reactance. When the cross-modal coupling is ignored, the coupled system resonates where the total reactance vanishes. Note that the frequency range shown in this figure is larger than the interaction-free range discussed at the end of Sec. III.

Figures 5(a) and (b) show that the first mode is rather stiff for very low frequencies mainly due to the cavity reflection effect. But the stiffness domination continues beyond the first *in vacuo* mode frequency due to the radiation stiffness. For a piston or a compact surface to radiate sound into an open space with or without baffle, the radiation reactance is normally positive, i.e., there is virtual mass from the surrounding air. But the situation for sound radiation in a duct is different. The opposite wall causes a mirror effect, and part of the radiation resistance is transformed into negative radiation mass or positive radiation stiffness (Huang, 2000). In such case, it makes more sense to regard this part of reactance as negative mass since its frequency dependence is inertialike [see the initial segment of the dashed line in Fig. 5(a)]. This mass can cancel out the structural mass, the former being larger in amplitude in the current example. This observation leads us to the conclusion that the structural mass is not important at all for the first mode response at low frequencies. The very high stiffness in the low-frequency range also indicates that the first mode cannot be relied upon for sufficient membrane reflection of the grazing incident sound. The total reactance is shown in Fig. 5(b). The first membrane mode now occurs at $f=0.189$, which is beyond the second *in vacuo* mode frequency. Another zero point can be found in Fig. 5(b) beyond $f=0.25$. The two resonance points found in Fig. 5(b) roughly correspond to the two peaks of $|V_1|$ shown on the right-hand edge of Fig. 4(1a). The qualifying word roughly is used here to indicate the lack of cross-modal coupling between the first and third mode. Again, if there was no cross-modal interactions, the first cavity mode at $f=0.2$ should have caused the membrane to have zero first mode response. The fact that this is not the case is shown in Fig. 4(1a).

Since $|V_4|$ is very small for $f<0.1$, the cross-modal coupling between the second and the fourth mode occurs strongly only beyond $f=0.1$. It is sufficient to analyze the reactance of the second mode alone in Figs. 5(c) and (d). Here, the cavity mode at $f=0.1$ indeed eliminates the second mode resonance, as shown in Fig. 4(1b). For $f<0.1$, both radiation and cavity reflection reactance are masslike, leaving the structural stiffness to dominate the coupled membrane response. The frequency of the second *in vacuo* mode, $f=0.138$, is shifted to $f=0.0515$ due to fluid added mass. This frequency corresponds to the peak of second mode response shown in Fig. 4(1b). This peak is higher than the first mode response in this region, shown in Fig. 4(1a), but its effectiveness in reflecting sound is not as good, cf. Figs. 4(2a) and (2b). The contribution towards sound reflection match in magnitude only beyond the second mode peak, see Figs. 4(3a) and (3b), where satisfactory overall performance of the membrane can be expected. It is therefore very important to determine analytically the second mode resonance.

B. Second mode resonance

For the second mode, $j=2$, θ in $[(j\pi)^2-\theta^2]$ can be ignored for a rough estimate without loss of qualitative information. The impedance Z_{22} given in Eq. (33), and the incident wave coefficients, I_2 given in Eq. (23), are approximated as follows:

$$4\pi^2 Z_{22}\approx(4L)(1-\cos\theta)+i(L_c+2L)[2\sin\theta+\theta]+iL_c 2(1-\cos\theta)\tan(\Theta/2),$$

$$I_2\approx\frac{1}{\pi}e^{i\theta/2}(1-e^{-i\theta}).$$

The second mode response is found to be

$$\begin{aligned} V_2&\approx\frac{-I_2}{Z_{22}+\mathcal{L}_2}=\frac{-i4\pi L^{-1}}{8\sin(\theta/2)+iX},\\ X&=(h_c^{-1}+2)[4\cos(\theta/2)+\theta/\sin(\theta/2)]\\ &\quad+4h_c^{-1}\sin(\theta/2)\tan(\Theta/2)\\ &\quad+(2\pi/L)^2[m\theta-T4\pi^2/\theta]/\sin(\theta/2). \end{aligned}\tag{34}$$

A weak resonance occurs when the amplitude of the denominator approaches a minimum, and this minimum can be shown to be approximately where the reactance term X in the denominator vanishes. By assuming a vanishing θ, and that Θ is also rather small even if it's larger than θ, the approximated resonance condition $X=0$ can be simplified as

$$[6(h_c^{-1}+2)8(\pi/L)^2(m-T4\pi^2/\theta^2)]\approx 0,$$

so that

$$f_{2\,\mathrm{res}}\approx\frac{gv}{2\pi L}=\frac{1}{L}\sqrt{\frac{T}{3(2+h_c^{-1})(L/2\pi)^2+m}}.\tag{35}$$

For the example in which $T=0.475$, $m=1$ and $L_c=L=5$, $f_{2\,\mathrm{res}}$ is found by this formula to be $f_{2\,\mathrm{res}}\approx 0.0533$, while the accurate root for $X=0$ is $f_{2\,\mathrm{res}}=0.0504$. Note that $\theta=0.5$ is not so small, but somehow the errors cancel themselves out coincidentally. Note also that X here only accounts for the plane wave contribution, which differs slightly from the full reactance shown in Fig. 5(d). Although the optimal value of T depends on L and m, it can be observed that the membrane length is the most influential parameter for the second mode resonance frequency.

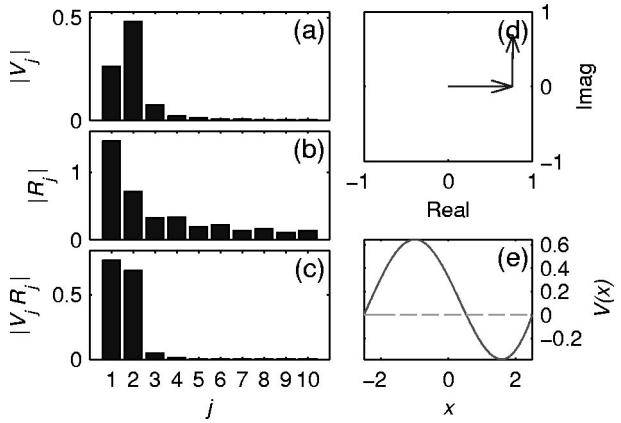

FIG. 6. Performance of the first peak at $f=0.06$, P1. (a) shows the velocity amplitude of each mode, $|V_j|$. (b) is the amplitude of the modal reflection coefficient, $|R_j|$. (c) is the sound reflection by each mode alone, $|V_jR_j|$. (d) shows how the complex modal contributions add up. (e) is the real (solid line) and imaginary (dashed line) parts of the membrane vibration velocity distribution, $V(x)$.

C. Peak performance points

The interference patterns of the first three peaks shown in Fig. 3(a), P1, P2, and P3, are analyzed as follows. Figure 6 is for P1 at $f=0.06$. The amplitudes of V_j, R_j, and V_jR_j are shown in Figs. 6(a), (b), and (c), respectively. The first mode proves more difficult to excite than the second, but the first mode is more effective in reflecting sound, $|R_1|>|R_2|$. As a result, the amplitudes of V_1R_1 and V_2R_2 are about equal. As shown in Fig. 6(d), the contributions from the two modes are nearly out-of-phase, hence no interference. The resultant membrane vibrations are, however, almost in-phase over the entire length as there is almost zero imaginary part in $V(x)$ shown in Fig. 6(e). The vibration is approximately described by $\sin(\pi\xi)+1.84\sin(2\pi\xi)$, which appears to be a distorted second mode with the left half-length extended and the right half-length reduced.

The modal contributions and their interference for P2 at $f=0.1$ are shown in Fig. 7. Here, the second mode proves almost impossible to excite since there is a first cavity mode, as explained by the divergence of the cavity reflection impedance in Eq. (21). The result is an in-phase combination of the first and the third mode in the form of $\sin(\pi\xi)$ $-1.50\sin(3\pi\xi)$. At this frequency, the third mode is not effective in reflecting sound. So that the only contribution towards reflection comes from the first mode. The reason why the first and third modes are excited so much at the cavity mode is that the cavity stiffness vanishes at this frequency, see the term $\tan^{-1}(\Theta/2)$ in Eq. (32), where $\Theta=\pi$ for this cavity mode.

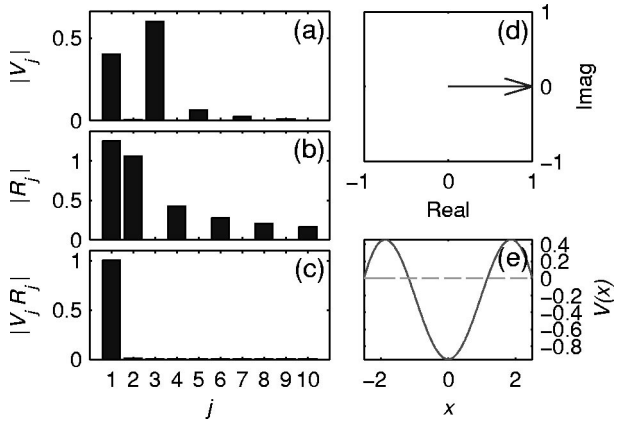

FIG. 7. The response of the membrane at the second peak of $f=0.102$, P2, cf. caption of Fig. 6.

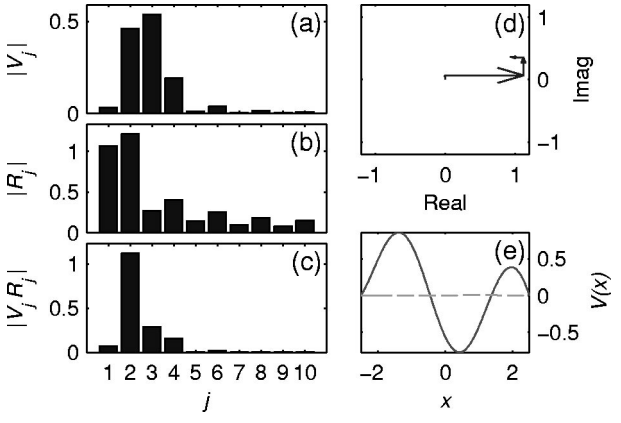

FIG. 8. The response at the third peak at $f=0.125$, P3, cf. caption of Fig. 6.

The third peak at $f=0.127$, P3, is analyzed in Fig. 8. In this case, the first mode is almost absent. The presence of the second and third modes is almost equally strong. The two modes are roughly in phase and the vibration velocity can be approximated by $\sin(2\pi\xi)+1.17\sin(3\pi\xi)$. Sound reflection mainly derives from the second mode, which is only slightly cancelled out by that from the fourth mode. The strong action by the second mode is caused by the increase in both the strength of the incident wave, I_2, and the modal reflectivity coefficient R_2, the two being related by $R_2=I_2L/4$. The excitation of the second mode vanishes when the incident wave coincides with the wavelength of the first mode, or the first cavity mode discussed above, which is $f=0.1$ in this case. As f moves away from this value, I_2 increases, as shown in Fig. 4(2b), and the stiffness term in Z_{22} reduces rapidly, as shown in Fig. 5(d).

V. CONCLUSIONS

Three figures are central to the understanding of the modal response and interaction pattern. They are Figs. 3, 4, and 5. The following conclusions are drawn for the membrane performance in the order of increasing frequency.

(a) When the frequency is extremely low, say, $f=0.0165$, the cavity is compact. The cavity is very stiff to the first mode and imposes high mass load to the second. In other words, the air in the cavity is barely compressible to the volume-displacing mode. The vibration of the second mode is not affected by the incompressibility, but it suffers from two adverse factors: (1) it's acoustically ineffective in reflecting sound and it's not excited, and (2) it's structurally hard due to the curvature of the deformed membrane. The limited reflection by the second mode only serves to cancel out that from the first mode until beyond the frequency of its own resonance. It can be said that the response of the membrane is controlled by the cavity for the first mode, and by the structural properties for the second mode.

(b) As frequency gradually increases towards $f=0.05$, the response of the first mode increases mainly due to the rapid reduction of the cavity stiffness. Since the structure properties do not have much influence in the particular configuration studied in this article, it can be read from Fig. 5(b) that the total stiffness reaches a rather low level around $f=0.05$, or when the ratio of the membrane length to wavelength is $L^*f^*/c^*=fL=0.25$, i.e., a quarter wavelength. Further reduction in system stiffness is gradual as f goes beyond 0.05. The increase in the action of the second mode is even more rapid when f approaches 0.05 for two reasons. One is that the structure is less stiff, which is natural to all modes, and the other is that the excitation, I_2, increases rapidly. The fluid exerts only virtual mass on the second mode. As a result, the structural stiffness is balanced by the virtual mass. The fluid and structure are coupled on equal footing to bring out a second mode resonance. As the frequency increases, the interference pattern between the first mode reflection and the second mode interference has changed from one of cancellation at DC frequency to one of out-of-phase relationship. The first peak in transmission loss, P1, appears at a frequency slightly beyond the second mode resonance. The main feature during the frequency running up to P1 is that the cavity has released its grip on the first mode, and the fluid couples closely with the second structural mode.

(c) Between the first peak point P1 and the second peak point P2, the pattern of reflection wave noninterference between the first two modes is rather stable. The contribution from the first mode, γ_1, grows with frequency due to the continuous decrease in cavity effect, which seems to have overridden the adverse effect of the decreasing receptivity to incident waves. Without a detailed analysis, it is difficult to determine the effect of the cross-modal coupling between the first and third modes within this frequency range. The dominant feature within the range, however, is the declining contribution of the second mode contribution, γ_2, until it vanishes at P2 at $f=0.1$, where the second mode is totally prohibited by the first cavity mode. The trade-off between the declining γ_2 and the increasing γ_1 resulted in a dip which in this example is still above 10 dB. If γ_2 were to decline a little faster than it does, the dip could go below 10 dB, leaving the TL pattern as one of normal Helmholtz resonator in which the sharp resonant peak is isolated. In order to halt the pace of this decline, the increase in the total reactance $\mathrm{Im}(Z_{22}+\mathcal{L}_2)$, shown as the first branch curve in Fig. 5(d), should be as gradual as possible. Since Z_{22} is by and large a function of geometry, the structural property in $\mathcal{L}_2$ can be adjusted in order to prevent the dip to go too low.

(d) The events between the second and third peaks begin to involve the third and fourth modes. However, their contribution, γ_3 and γ_4, remain to be small. The second peak P2 features the solo action of the first mode, as explained earlier. The third peak is contributed to mainly by γ_2. The reason why γ_2 is gaining ground towards this frequency is that the second mode continues to gain receptivity to the incident sound, and it moves away from the banned region of the first cavity mode. Part of the reason why γ_1 disappears totally is that the modal response V_1 decreases in amplitude due to the poor modal receptivity, and partly due to the cross-modal interaction between the first and third modes, which is too involved to discuss in detail. There is also a dip between the two peaks, which is again determined by the trade-off between the declining γ_1 and increasing γ_2. The trade-off in this region is exactly opposite to what happens between P1 and P2, where γ_1 increases but γ_2 decreases. Overall, it is found that the actions of the first two modes are by and large supplementary to each other, a key element in sustaining a high TL over a broad frequency band.

The analyses so far have been conducted for one particular set of parameters listed in Eq. (30) for the purpose of in-depth understanding of the fluid-membrane coupling mechanism. A detailed parametric study has to be conducted before an actual design can be made. Without giving details of such a study, the following discussions are reported. First, the membrane tension plays a pivotal role in tuning the relative response of various axial modes and the positions of the peaks in the transmission loss spectrum as shown in Fig. 3. The choice of $T=0.475$ is made in such a way that the spectral troughs between P1 and P2 is roughly level with that between P2 and P3. The result is a balanced spectrum with a wide stopband. When the tension vanishes, it can be demonstrated that the response of the system is essentially a simple expansion chamber. When tension approaches infinity, the membranes do not vibrate at all as they become hard walls. An optimal tension exists and the value of such tension depends on the choice of the objective function in the optimization process. In the particular example given with a square duct of height 17 cm, the tension corresponding to $T=0.475$ is 1944N. The dimensional force obviously increases with h^{*2} when other dimensionless parameters are fixed, and the dimensional frequency for the stopband decreases in proportion to c_0^*/h^*. The ratio of the membrane length to the duct height, $L=L^*/h^*$, is also very important. When L is too short, one can expect a very ineffective second mode in receiving and reflecting long waves, see Eqs. (23) and (28). When L is too long, however, the method of traditional duct lining with an acoustically transparent membrane cover may become more attractive. Again, some optimal length exists for a specific design task.

ACKNOWLEDGMENT

The author thanks the Hong Kong Polytechnic University for its support through the research project G-YC93.

Cheng, L. (**1994**). ''Fluid-structural coupling of a plate-ended cylindrical shell: vibration and internal sound field,'' J. Sound Vib. **174**, 641–654.

Doak, P. E. (**1973**). ''Excitation, transmission and radiation of sound from source distributions in hard-walled ducts of finite length (I): the effects of duct cross-section geometry and source distribution space-time pattern,'' J. Sound Vib. **31**, 1–72.

Dowell, E. H., Gorman, G. F., and Smith, D. A. (**1977**). ''Acoustoelasticity: general theory, Acoustic natural modes and forced response to sinusoidal excitation, including comparisons with experiment,'' J. Sound Vib. **52**, 519–542.

Dowell, E. H., and Voss, H. M. (**1963**). ''The effect of a cavity on panel vibrations,'' AIAA J. **1**, 476–477.

Frommhold, W., Fuchs, H. V., and Sheng, S. (**1994**). ''Acoustic performance of membrane absorbers,'' J. Sound Vib. **170**, 621–636.
Fuchs, H. V. (**2001a**). ''From advanced acoustic research to novel silencing procedures and innovative sound treatments,'' Acustica **87**, 407–413.
Fuchs, H. V. (**2001b**). ''Alternative fiberless absorbers—new tools and materials for noise control and acoustic comfort,'' Acustica **87**, 414–422.
Guy, R. W. (**1979**). ''The response of a cavity backed panel to external airborne excitation: a general analysis,'' J. Acoust. Soc. Am. **65**, 719–731.
Horoshenkov, K. V., and Sakagami, K. (**2001**). ''A method to calculate the acoustic response of a thin, baffled, simply supported poroelastic plate,'' J. Acoust. Soc. Am. **110**, 904–917.
Huang, L. (**1999**). ''A theoretical study of duct noise control by flexible panels,'' J. Acoust. Soc. Am. **106**, 1801–1809.
Huang, L. (**2000**). ''A theory of reactive control of low-frequency duct noise,'' J. Sound Vib. **238**, 575–594.
Kang, J., and Fuchs, H. V. (**1999**). ''Predicting the absorption of open weave textiles and micro-perforated membranes backed by an air space,'' J. Sound Vib. **220**, 905–920.
Lyon, R. H. (**1963**). ''Noise reduction of rectangular enclosures with one flexible walls,'' J. Acoust. Soc. Am. **35**, 1791–1796.
Mechel, F. P. (**2001**). ''Panel absorber,'' J. Sound Vib. **248**, 43–70.
Pan, J., and Bies, D. A. (**1990**). ''The effect of fluid-structural coupling on sound waves in an enclosure—theoretical part,'' J. Acoust. Soc. Am. **87**, 691–707.
Pretlove, A. J. (**1965**). ''Free vibrations of a rectangular panel backed by a closed rectangular cavity,'' J. Sound Vib. **2**, 197–209.
Sum, K. S., and Pan, J. (**1998**). ''A study of the medium frequency response of sound field in a panel-cavity system,'' J. Acoust. Soc. Am. **103**, 1510–1519.